

Hollowness Effect and Entropy in High Energy Elastic Scattering

S. D. Campos*

*Departamento de Física, Química e Matemática,
Universidade Federal de São Carlos Sorocaba, São Paulo CEP 18052780, Brazil*

V. A. Okorokov†

*National Research Nuclear University MEPhI (Moscow Engineering
Physics Institute), Kashirskoe highway 31, 115409 Moscow, Russia*

(Dated: December 14, 2024)

This paper presents an explanation for the hollowness effect of the inelastic overlap function claiming that result is a consequence of fundamental thermodynamic processes. The use of Tsallis entropy allows the identification of energy in the center-of-mass system with the entropic index w . Moreover, the probabilities involved in the description of the Tsallis entropy are replaced by the inelastic overlap function, which represents the probability of an event in a given energy and impact parameter. The obtained entropy formula can be directly connected to the unitarity, imposing restrictions on the shape of the function. The Coulomb and confinement potential is considered as naive approaches to the internal energy of the colliding hadrons. The Coulomb potential for the impact parameter picture is not able to furnish any result near forward direction. However, the confinement potential results in the hollowness effect of the inelastic overlap function.

PACS numbers: 13.85.Dz

I. INTRODUCTION

The proton-proton (pp) and antiproton-proton ($\bar{p}p$) elastic scattering at high energies remains as one of the surprising open issues of collision processes. Nowadays these open questions may will be solved by the new phase of the so-called High Luminosity Large Hadron Collider (HL-LHC) which will deliver 3000 fb^{-1} of integrated luminosity [1]. Other questions then may arise allowing the construction or improving present day models.

As well-known the geometrical point of view of the pp and $\bar{p}p$ scattering is an important tool for the understanding of its dynamics, furnishing insights and approaches to the non-perturbative QCD. Of course, protons and antiprotons are not point-like objects, but at high energies they behave quite similar to the disk picture of classical optics as can be viewed in many experimental results over decades. However, recent experimental results and models indicate this picture is not accurate enough.

From the original hypothesis in [2, 3] showing a gray area occurring at the impact parameter value $b = 0 \text{ fm}$ results recently the idea of a hollowness effect [4], suggesting the presence of a minimum in the inelastic profile function at zero impact parameter. This unexpected result produces a series of explanations [2–11]. However, none of these explanations take into account the entropy associated to the elastic scattering in the impact parameter space. As shown in [12], the Tsallis entropy (TE) can be connected to the inelastic overlap function and to the energy critical value s_c associated with a phase transition in the total cross section data. This critical value divides the total cross section dataset into two regions of different fractal dimensions exposing the presence of a multifractal character of this physical quantity [13]. It is important to stress here that TE emerges exactly from the context of multifractal structures [14]. Therefore, its use for the present paper can be viewed as a natural application for the high energy pp and $\bar{p}p$ scattering.

On the other hand, the multifractal character also occurs to the transferred momentum space [15–20], reinforcing the necessity of the use of TE. Therefore, both multifractal characteristics in different variables should be noted in the impact parameter space, revealing some novel behavior present in the inelastic overlap function, for instance.

As well-known, entropy is one of the most important physical quantities of physics. Actually, it is the time arrow and therefore it can be taking into account in any physical explanation of scattering since there is an obvious two-stage process: before the scattering and after the scattering. In the middle there are models trying to explain what is occurring. The self-organization of the internal constituents of the hadron during the collision process can interfere in

*Electronic address: sergiadc@ufscar.br

†Electronic address: VAOkorokov@mephi.ru; Okorokov@bnl.gov

what is measured. Of course, the repeatability of such process turns predictable, some aspects of the elastic scattering.

The use of entropy poses a novel problem: the internal energy of the process. This is a very hard question and presently unsolved. As a naive first glance, one proposes the use of two potentials for different physical approaches. The first one is the use of the Coulomb potential replacing the internal energy of the hadron. The obvious consequence is the elastic scattering of pp and $\bar{p}p$ being treated as billiard balls scattering. Of course, this potential is unable to present any information about the internal structure of the hadrons. However, due approximations done, any information near forward direction are forbidden (to some $b < b_{\min}$). The second approach uses the confinement potential. Contrary to the first one, this potential allows a view on the internal arrangement of quarks and gluons manifested in the impact parameter space. The consequence we claim here is the emergence of the hollowness effect near forward direction.

The paper is organized as follow. In section II one sets the problem. In section III one presents both potentials used to simulate the internal energy of pp and $\bar{p}p$. Section IV presents the discussions and conclusions.

II. HOLLOWNESS EFFECT AND ENTROPY

The high energy pp and $\bar{p}p$ elastic scattering can be analyzed by using both the transferred momentum q^2 and the impact parameter b inasmuch as these variables are connected with a Bessel transform. Therefore, the physical constraints on one space can be rewritten in the other one sometimes revealing details or furnishing insights to solve a problem.

The impact parameter space is the geometrical point of view of the elastic scattering and possess a clear classical appeal. In this sense, the disk picture is naturally used to describe pp and $\bar{p}p$ elastic scattering. The elastic scattering amplitude $F(s, q^2)$ is written by using the impact parameter as

$$F(s, q^2) = i \int_0^\infty b db J_0(qb) \{1 - \exp[i\chi(s, b)]\} = i \int_0^\infty b db J_0(qb) \Gamma(s, b), \quad (1)$$

where \sqrt{s} is the collision energy in the center-of-mass system, $J_0(x)$ is a zeroth order Bessel function, and $\chi(s, b)$ is the eikonal function written as

$$\chi(s, b) = \text{Re}\chi(s, b) + i\text{Im}\chi(s, b), \quad \text{Im}\chi(s, b) \geq 0, \quad (2)$$

where the imaginary part corresponds to opacity function related to matter distribution inside the incident particles. The profile function $\Gamma(s, b) = \text{Re}\Gamma(s, b) + i\text{Im}\Gamma(s, b)$ is the elastic scattering amplitude in the impact parameter space to a fixed s and can give an estimate of the interacting particle sizes and an analysis of their internal structure. Moreover, the unitarity condition can be written by using the inelastic overlap function as

$$0 \leq G_{\text{inel}}(s, b) = 2\text{Re}\Gamma(s, b) - |\Gamma(s, b)|^2 \leq 1, \quad (3)$$

that represents the probability of absorption associated with a specific (s, b) pair and one expects as one moves away from the forward collision ($b = 0$) the interaction probability diminishes. The general belief is that at $b = 0$ and to a sufficient high energy $G_{\text{inel}}(s, 0) \rightarrow 1$ implying that to $s \rightarrow \infty$ all pp and $\bar{p}p$ presents the same physical behavior near the forward direction.

Several theorems started to be proved from the 1960's and some of them established the fundamental basis of theoretical understanding of high energy elastic scattering. For instance, the elastic to total cross section ratio is one of these remarkable results obtained from well-established basis [21–25]. The detailed analysis of this cross section ratio in nucleon-nucleon collisions [26] shows that at high energies the approximate relation

$$\sigma_{\text{el}}(s)/\sigma_{\text{tot}}(s) \approx 1/4 \quad (4)$$

is valid in pp up to the highest experimentally reached energy $\sqrt{s} = 57$ TeV within large errors for this point.

The unitary equation (3) can also be written as

$$G_{\text{inel}}(s, b) = \text{Re}\Gamma(s, b)[2 - \text{Re}\Gamma(s, b)] - \text{Im}^2\Gamma(s, b). \quad (5)$$

The above expression can be rewritten by taking into account derivative dispersion relations and the crossing property over $\text{Im}\Gamma(s, b)$. Notice that derivative contributions depend on the transferred momentum involved, i.e., when $q^2 \rightarrow 0$ the derivative terms contribution occurs to the periphery of the collision and when $q^2 \rightarrow \infty$ the contribution is central. Therefore, the expression (5) possess two regimes depending on b is central or peripheral. Considering large values of b , $\text{Im}\Gamma(s, b) \approx \text{Re}\Gamma(s, b)$ and, therefore, derivative terms should be taken into account.

However, to small values of b , then $\text{Im}\Gamma(s, b) \ll \text{Re}\Gamma(s, b)$ and derivative terms can be neglected. Thus to small values of b one writes near forward direction

$$G_{\text{inel}}(s, b) \approx \text{Re}\Gamma(s, b)[2 - \text{Re}\Gamma(s, b)], \quad (6)$$

and one can identify $1 \leq \text{Re}\Gamma(s, b) \leq 2$, where $\text{Re}\Gamma(s, b) = 2$ is the completely non-absorptive case and $\text{Re}\Gamma(s, b) = 1$ is the full absorptive case. Taking the partial derivative with respect to b of (6), then one writes ($\partial_x \equiv \partial/\partial x$)

$$\partial_b G_{\text{inel}}(s, b) \approx 2\partial_b \text{Re}\Gamma(s, b)[1 - \text{Re}\Gamma(s, b)]. \quad (7)$$

Note that at some critical value b_c , the $\partial_b G_{\text{inel}}(s, b)|_{b=b_c} = 0$ can be achieved if $\partial_b \text{Re}\Gamma(s, b)|_{b=b_c} = 0$ and/or $\text{Re}\Gamma(s, b_c) = 1$. The *and* connective means that b_c is a critical value and the process is completely absorptive at b_c . On the other hand, the *or* case can be analyzed as follows. If $\partial_b \text{Re}\Gamma(s, b)|_{b=b_c} = 0$ but not $\text{Re}\Gamma(s, b_c) = 1$, then b_c is a critical value but does not represent the full absorptive case, i.e., the inelastic overlap function does not represent a black disk to b_c . On the contrary, the full absorptive case does not represent a critical point of $\text{Re}\Gamma(s, b)$. This can be considered the non-physical case since the inelastic overlap function is limited and achieves its maximum or minimum at the ending point. Therefore, there are two situations able to furnish a zero to $\partial_b G_{\text{inel}}(s, b)$ at some critical value of the impact parameter $b = b_c$. The first situation can be achieved by considering that at $b = b_c$ the $\partial_b \text{Re}\Gamma(s, b)|_{b=b_c} = 0 \cap \text{Re}\Gamma(s, b_c) = 1$, hence b_c is a critical value and represents the full absorptive case. The second situation can be achieved if $\partial_b \text{Re}\Gamma(s, b)|_{b=b_c} = 0 \cap \text{Re}\Gamma(s, b_c) \neq 1$.

Taking into account the allowable range of $\text{Re}\Gamma(s, b)$ the sign of $\partial_b \text{Re}\Gamma(s, b)$ determines the sign of $\partial_b G_{\text{inel}}(s, b)$: considering $\partial_b G_{\text{inel}}(s, b) > 0$, then the only possible physical result is $\partial_b \text{Re}\Gamma(s, b) < 0$ and vice versa. Therefore, the sign of $\partial_b G_{\text{inel}}(s, b)$ is controlled only by the sign of $\partial_b \text{Re}\Gamma(s, b)$ and the inelastic overlap function change its sign according to b (fixed s). As stated above $\text{Re}\Gamma(s, b)$ is connected to the imaginary part of $F(s, q^2)$ and changes in the sign of $\text{Im}F(s, q^2)$ also represents a change in the sign of $\text{Re}\Gamma(s, b)$. As well-known, $\text{Im}F(s, q^2)$ oscillate according to q^2 and, therefore, the sign of $\partial_q \text{Im}F(s, q^2)$ changes.

On the other hand, one can analyze the behavior of $G_{\text{inel}}(s, b)$ by using the TE. First of all, there are several ways to compute the entropy of a thermodynamic system being the usual the well-known Boltzmann entropy. This entropy is usually defined to a system of non-interacting particles. Hence, this entropy is additive: the entropy of the whole system is the sum of the entropy of each subsystem. However, a system with interacting subsystem (sometimes strongly correlated) needs an entropy calculation that takes it into account since hadrons are composed of strongly interacting particles (gluons and quarks). The TE naturally can be applied for this situation since it is non-additive. Moreover, Rényi entropy [27], Shannon entropy [28], Abe entropy [29] and Boltzmann entropy, for instance, can be reduced to TE [30, 31]. Furthermore, TE possess two (among others) interesting mathematical properties: it is concave for all $w > 0$, a crucial characteristic for an entropy function and it obeys the Lesche–stability condition, ie, it is stable under small perturbations of probabilities. Therefore, the use of TE can furnish a description of the physical system under study.

The entropic index- w of the TE is replaced by the energy s [12]

$$w = s/s_c, \quad (8)$$

where s_c is the critical value associated to the BKT-like phase transition [12] present in the fractal structure of the total cross section [13]. Therefore, w plays the physical role of a transition parameter at each s considered. When $s > s_c$, the fractal dimension is positive and negative when $s < s_c$, ie, the TE possess two behaviors depending on $w > 1$ or $w < 1$ as seen along the text. On the other hand, as noted in [13], the negative fractal dimension measures the emptiness of the hadron (the slow down part of the total cross section data); the positive fractal dimension can be associated to the usual measure of the total cross section (the growing part of the total cross section data).

In [12] the TE is related to the scattering at fixed s by means of the inelastic overlap function $G_{\text{inel}}(s, b)$, due to non-elastic s -channel intermediate states as ($k \equiv s/s_c - 1$)

$$S_T \equiv S_T(s, b) = k^{-1}[1 - G_{\text{inel}}(s, b)]. \quad (9)$$

It is interesting to note that unitarity demands $0 \leq G_{\text{inel}}(s, b) = 1 - kS_T \leq 1$ implying the replacement $kS_T \rightarrow \tilde{S}_T$, where \tilde{S}_T is the normalized entropy.

As well-known, the inelastic overlap function take into account all the intermediate inelastic channel contributions. Therefore, the entropy (9) can be associated with the inelastic scattering contributions. In the above result if $G_{\text{inel}}(s, b) \rightarrow 1$ (the black disk limit) then $S_T \rightarrow 0$. The physical meaning of this result is simple: at the black disk limit the system (the motion of the internal constituents) is in its lowest possible value, as stated by Quantum Mechanics. Therefore, the system tends to be well-defined in the sense that its physical state is well-known.

On the other hand, the inelastic overlap function is interpreted as the probability of an elastic scattering in a given (s, b) . Therefore, $G_{\text{inel}}(s, b) = 1$ implies that at head-on collision $b = 0$ (or at some $b \neq 0$), the probability achieves its maximum as well as the entropy tends to the minimum. It does not mean that the entropy is zero everywhere inside the hadron. In general, the belief is that at $s \rightarrow \infty$, the black disk limit is achieved at $b = 0$. However, it is not necessarily true since one possesses a change in the sign according to s/s_c . To see this, observe that the partial derivative of S_T with respect to b is given by

$$\partial_b S_T = -k^{-1} \partial_b G_{\text{inel}}(s, b). \quad (10)$$

Assuming $s > s_c$ (high energy regime), then the sign of $\partial_b S_T$ is determined by the sign $\partial_b G_{\text{inel}}(s, b)$. In this regime, the fractal dimension of the total cross section is positive representing the increase in matter density inside the hadron [13]. Therefore, according to the above analysis, b_c determines a region inside of the hadron where the entropy increases ($b > b_c$) or decreases ($b < b_c$). On the other hand, considering $s < s_c$ (low energy regime), the existence of b_c implies in an increasing ($b < b_c$) or decreasing ($b > b_c$) entropy. The fractal dimension of the total cross section is negative and represents the emptiness of the hadron or the absence of a well-defined internal structure [13]. The same results can be obtained replacing (7) in to (10) showing that matter distribution of the hadron according to existence of b_c determines the entropy behavior.

III. INTERNAL ENERGY AND EFFECTIVE POTENTIAL

As well-known, the total internal energy U of a hadron cannot be deduced by using the first principles of thermodynamics. One assumes here, as a first approximation, that U is a function of the *effective* potential \tilde{V} , thus $U \approx U(\tilde{V})$. Of course, this first approximation excludes the kinetic term and the action due to external forces, but the approximation seems in agreement with calculations within T -matrix approach [32] at least on the qualitative level.

According to stated in the preceding section, one replaces kS_T by its normalized form since $G_{\text{inel}}(s, b)$ obey the unitarity condition. Therefore, the entropy of the above system can also be written by using the thermodynamics assuming small variations on the hadron volume and constant number of particles-constituents in the system as

$$\partial_U \tilde{S}_T = \tilde{T}^{-1}, \quad (11)$$

where \tilde{T} is the normalized temperature, $\tilde{T} \equiv T/k$. According to [12], $\tilde{T} = \pm 1$, depending on $s > s_c$ (+1) or $s < s_c$ (-1). In general one can suggest the following equation

$$G_{\text{inel}}(s, b) = 1 - \tilde{V}(s, b), \quad (12)$$

within the potential approach, where $\tilde{V}(s, b)$ can be obtained with help of some procedure from the potential $V(s, b)$. Taking into account the unitarity condition (3) it should be $0 \leq \tilde{V}(s, b) \leq 1$ and, consequently, the normalization can be suggested as such procedure with the specific details depended on view and behavior of the $V(s, b)$ in the kinematic region under study. It should be noted some restricted ranges of impact parameter ($b_{\min} \leq b \leq b_{\max}$) and collision energy ($s_{\min} \leq s \leq s_{\max}$) are considered in reality with finite values of boundaries $b_{\min/\max}$, $s_{\min/\max}$. The following general statement can be obtained from (12): the black disk regime $G_{\text{inel}}(s, b) \rightarrow 1$ is reached only if $\tilde{V}(s, b) \rightarrow 0$ in some kinematic domain and / or separate points of the (s, b) plane.

Then within potential approach one can obtain

$$\tilde{S}_T(s, b) = \tilde{V}(s, b) \quad (13)$$

replacing (12) into the relation (9). Consequently the b -dependence of the TE is the same as for effective potential $\tilde{V}(s, b)$. In general, the s -dependence of the S_T for certain types of the potential $V(s, b)$ can be deduced with the help of the (13) and k in accordance with the definition of the normalized TE at appropriate choice of the parameters like s_c etc. In addition one can note that the equation (13) is in agreement with the (11).

Although there is no potential able to describe the elastic scattering in this regime, one considers here two potentials as an attempt to explain the behavior of the inelastic overlap function. The first is the usual Coulomb potential in terms of the impact parameter b allowing a naive view of the inelastic overlap function of the hadron outside. From the hadron inside, the use of the confinement potential allows us the point of view of the internal constituents.

A. Coulomb Potential

In this first glance, one assumes that hadron scattering can be approximated by the Coulomb potential which implies in assuming the hadrons as point-like particles. Despite this approach is very naive, it can furnish at least a classical picture of the inelastic overlap function. Assuming $r = |\mathbf{r}_i - \mathbf{r}_j|$ as the distance between the hadrons placed at \mathbf{r}_i and \mathbf{r}_j and $m^2 \ll s$, then using the impact parameter b one can approximate the Coulomb potential $V_C(r) = -a/r$ at fixed s by

$$V_C(r) \approx V_C(s, b) = -ab^{-3}(b^2 - 2/s). \quad (14)$$

Here $a > 0$ is a dimensionless parameter corresponding to the electrostatic interaction of the pair, $b = r \cos \theta$, where θ is the angle between \mathbf{b} and \mathbf{r} [33]. Fig. 1 shows the b - (a) and the s -dependence (b) for exact view of Coulomb potential and its approximation in the impact parameter space (14). In the last case the curves are shown for the fixed $\sqrt{s} = 31.0$ and 52.8 GeV (Fig. 1a) and for the fixed $b = 0.01$ and 0.02 fm (Fig. 1b). The approximation done above is better for the peripheral collision since $V_C(s, b) \rightarrow V_C(r)$ to $b \rightarrow \infty$ and $r \rightarrow \infty$ as shown in Fig. 1a¹. The minimum of the $V_C(s, b)$ is placed at $b_{\min} = \sqrt{6/s}$, $V_C(s, b_{\min}) = -a\sqrt{2s/27}$ which roughly means that considering $b \gtrsim b_{\min}$, $V_C(s, b) \simeq V_C(r)$ as seen in Fig. 1a. Therefore, the approximation in (14) can be used to $b > b_{\min}$ and information about $b \rightarrow 0$ is forbidden, i.e. any information obtained to $V_C(s, b < b_{\min})$ may not correctly describe the elastic scattering in the impact parameter point of view. At given b one can expect that the approximate function $V_C(s, b)$ will reasonably agree with curve for exact Coulomb potential at $s > s_{\min}$ and this agreement will improve with future growth of the collision energy, where $\sqrt{s_{\min}} = \sqrt{6}/b$ for fixed b . This statement is confirmed in Fig. 1b: the range of \sqrt{s} for coincidence between curves for $V_C(r)$ and $V_C(s, b)$ expands down on the smaller collision energies with growth of the b .

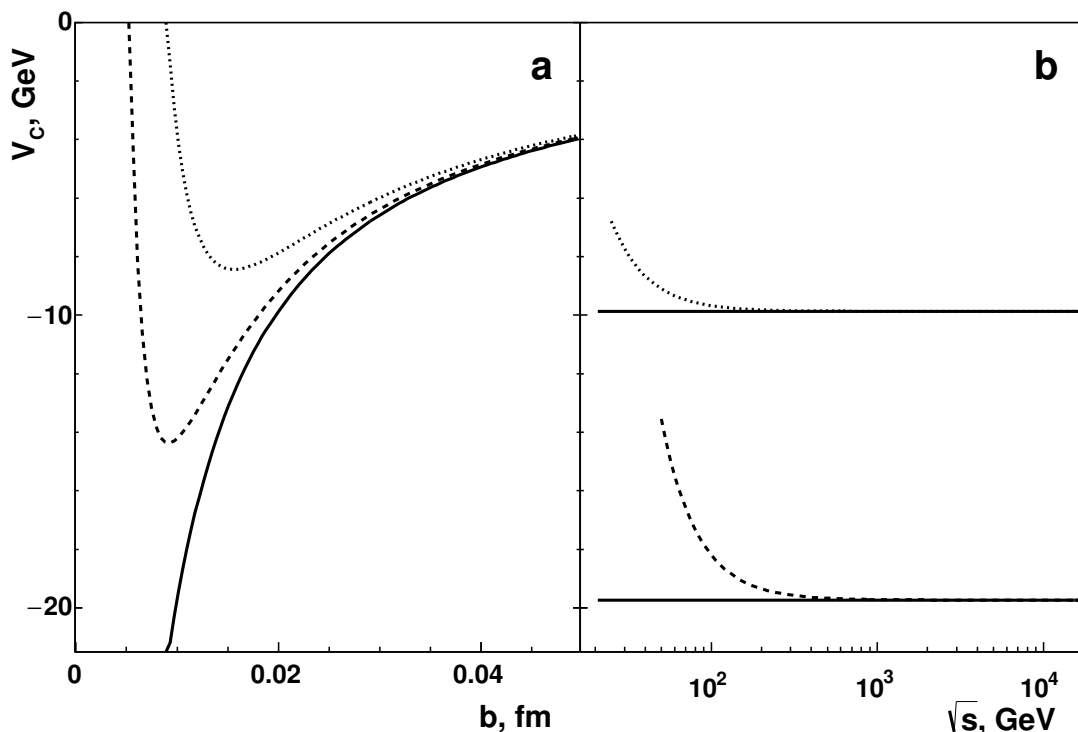


FIG. 1: Dependence of the exact view of Coulomb potential (solid lines) and approximate relation (14) on impact parameter (a) and collision energy (b): a – the dotted line corresponds to the approximation (14) at $\sqrt{s} = 31.0$ GeV and the dashed line – to the (14) at $\sqrt{s} = 52.8$ GeV; b – the dotted curve is the approximation (14) at $b = 0.02$ fm and the dashed line – the (14) with $b = 0.01$ fm. The values $a = 1$, $\theta = 0$ are used in approximate view of the $V_C(r)$ for the sake of simplicity.

¹ We are not interested here in the description of the tail of the inelastic overlap function. Therefore, we do not take into account derivative terms.

As it is known, the Coulomb potential is the long-range one and $\forall r : V_C(r) < 0$, consequently, $V_C(s, b) < 0$ at any b and s . For potential with constant sign the following normalization can be used

$$\tilde{V}(s, b) = [V^{\max}(s, b)/V(s, b)]^m, \quad (15)$$

where $V^{\max}(s, b)$ is the potential maximum, $m = \pm 1$ with up (down) sign for negative (positive) values of $V(s, b)$ within whole range of values of the kinematic parameter under consideration. Therefore, one writes

$$G_{\text{inel}}^C(s, b) = 1 - \tilde{V}_C(s, b) = 1 - \frac{b}{b_{\max}} \frac{1 - 2/sb_{\max}^2}{1 - 2/sb^2}, \quad (16)$$

where $\tilde{V}_C(s, b)$ is the effective (normalized) Coulomb potential defined by (15) with $m = 1$ and $V_C^{\max}(s, b) \equiv V_C(s, b_{\max})$ due to negative values and smooth behavior of the $V_C(s, b)$ in Fig. 1. Here b_{\max} is the appropriate value for high boundary of b within the certain issue and the general condition $b_{\min} \ll b_{\max}$ is used for evaluation of the b_{\max} in the present paper. The detailed study above (Fig. 1) assumes that $G_{\text{inel}}^C(s, b)$ defined by (16) can describe only the region $b \geq b_{\min}$, at fixed s and the range $s \geq s_{\min}$ at fixed b within approach the hadrons as point-like particles. The approximate relation

$$\tilde{V}_C(b) \approx b/b_{\max} \quad (17)$$

is applicable for $b > b_{\min}$ in the kinematic domain of validity of the condition $sb^2 \gg 2$. Here almost energy-independent behavior of $G_{\text{inel}}^C(s, b)$ is expected in almost whole allowed range $b \in [b_{\min}, b_{\max}]$ with exception of the narrow region close to the low boundary. The (very) weak dependence on $G_{\text{inel}}^C(s, b)$ on \sqrt{s} can be remained due to approximate view of the relation (17) and the range of such behavior of $G_{\text{inel}}^C(s, b)$ can be expanded to larger b with the increase of the boundary value b_{\max} .

Fig. 2 shows the behavior of the inelastic overlap function in dependence on the impact parameter for the certain b_{\max} and several collision energies from the low-boundary one which is the minimum allowable energy for nucleon-nucleon scattering $\sqrt{s_{\text{l.b.}}} = 2m_p$ up to the nominal energy for pp mode at the LHC, where m_p is the proton mass [34]. The choice $b_{\max} = 1$ fm is due to the typical linear scale of hadron physics. As seen the $G_{\text{inel}}^C(s, b)$ is characterized by almost flat behavior at small $b \lesssim 0.1$ fm with consequent fast decreasing as b growth for energy range $\sqrt{s} \gtrsim 14$ GeV. Such behavior may be associated with the absence of an internal structure combined with the naive potential description. The region of the weak changing of $G_{\text{inel}}^C(s, b)$ narrows with decreasing of the collision energy. This statement is confirmed by inner panel (Fig. 2) shown the region of the visible difference between two curves $G_{\text{inel}}^C(s, b)$ at $\sqrt{s} = 52.8$ GeV (dashed line) and $\sqrt{s} = 14$ TeV (dot-dashed line). These features of the behavior of $G_{\text{inel}}^C(s, b)$ are in full accordance with a detailed analysis of the relation (17). It is interesting to note that in the approach of point-like hadrons as the collision energy increases the $G_{\text{inel}}^C(s, b)$ shown in Fig. 2 extends to very small values of b . Furthermore the behavior $G_{\text{inel}}^C(s, b)$ corresponds to the black disk approach at $b_{\min} < b \lesssim 0.10$ fm and there is no signatures for hollowness effect at any \sqrt{s} under discussion. At $\sqrt{s} \lesssim 14$ GeV the inelastic overlap function decreases with the increasing of b in an almost whole allowed range of the impact parameter. The $G_{\text{inel}}^C(s, b)$ is significantly smaller 1.0 and black disk approach is not valid in the energy range $\sqrt{s} \lesssim 14$ GeV.

The b -dependence of the TE for Coulomb potential can be immediately derived from the Fig. 2 and relation (16). At qualitative level the normalized TE for scattering on the Coulomb potential $\tilde{S}_T^C(s, b)$ is characterized by very small values of $b_{\min} < b \lesssim 0.10$ fm with future fast growth and $\tilde{S}_T^C(s, b) \rightarrow 1$ at large enough impact parameter values $b \sim b_{\max}$, i.e. for peripheral collisions.

In accordance with general way the s -dependence of the TE for Coulomb potential is deduced by substituting the (16) into the relation (9) at $\sqrt{s_c} = 25$ GeV and $b < b_{\max} = \varepsilon_1 b_{\min}$, where the $\varepsilon_1 = 10$ and b_{\min} is defined by $s_{\text{l.b.}}$ in order to (i) the condition $b_{\min} \ll b_{\max}$ be correct and (ii) the whole energy range be available for calculation at certain b . Detailed analysis of (9) shows that the k defines the sign of the $S_T^C(s, b)|_{b=b_{\text{fixed}}}$, the quantity demonstrates the sharper behavior as the s approaches to the critical value s_c , furthermore the absolute values of the TE for $s < s_c$ ($|S_T^C| = -S_T^C$) are larger by orders than that for $s > s_c$ ($|S_T^C| = S_T^C$). Therefore the $|S_T^C|$ seems more adequate quantity for study of s -dependence of the TE for the approximation (14) of the Coulomb potential in b -space. The energy dependence on the $|S_T^C|$ is shown in Fig. 3 for several values of b at parameter values chosen above. As expected the $|S_T^C|(s)$ is characterized by the sharp behavior close to the critical energy s_c with a subsequent smoother decrease. The $|S_T^C|$ aspires to the finite values at $s \rightarrow s_{\text{l.b.}}$ in the energy domain $s < s_c$, on the other hand the absolute value of the TE (9) for the Coulomb potential decreases significantly with the growth of collision energy for $s > s_c$ (Fig. 3). The energy dependence on $|S_T^C|$ is mostly defined by the k -factor, the influence of the $\tilde{V}_C(s, b)$ is weak and it only manifests itself at low and intermediate energies: at low boundary $s_{\text{l.b.}}$ the relative difference between the exact $\tilde{V}_C(s, b)$ and the s -independent approximation (17) is about 9% for $b = 0.5$ fm and $\simeq 0.7\%$ for $b = 1.5$ fm;

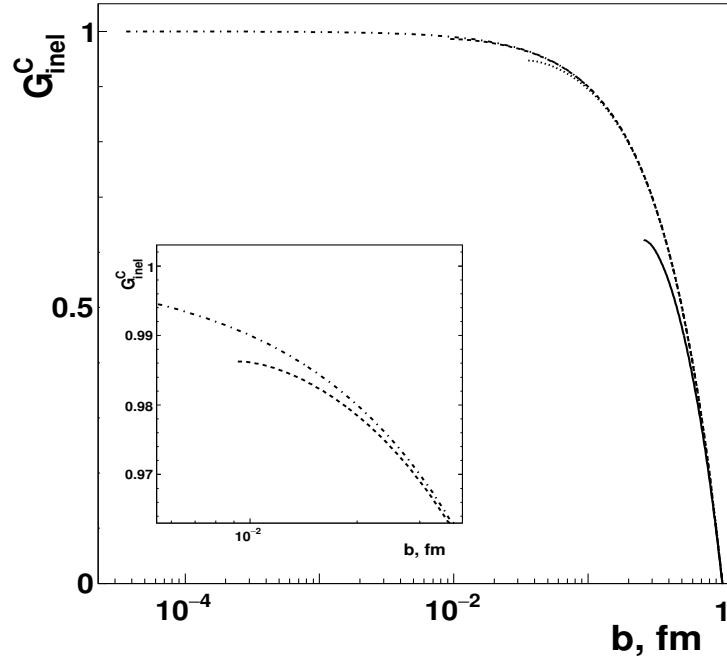


FIG. 2: Behavior of $G_{\text{inel}}^{\text{C}}(s, b)$ using the Coulomb potential, where the full line considers $\sqrt{s_{\text{l.b.}}} \approx 1.88$ GeV, dotted one $\sqrt{s} = 13.8$ GeV, dashed curve $\sqrt{s} = 52.8$ GeV and dot-dashed line $\sqrt{s} = 14$ TeV. In all case the curves are obtained considering approximation (14) and $b_{\text{min}} \leq b \leq b_{\text{max}}$ with $b_{\text{max}} = 1.0$ fm. Inner panel: the region of the visible difference between two curves at $\sqrt{s} = 52.8$ GeV and $\sqrt{s} = 14$ TeV.

furthermore this difference decreases fast with energy growth and it is negligible ($< 0.5\%$) at $\sqrt{s} \lesssim 8$ GeV for any b under consideration.

As well-known, the Coulomb scattering treats the hadrons as billiard balls and does not take into account the influence of the internal arrangement of quarks and gluons to the complete description of the total cross section (and any other observable). Therefore, any treatment of the elastic scattering should take into account quarks and gluons which may avoid the occurrence of b_{min} or presents an explanation of what occurs to $b < b_{\text{min}}$.

B. Confinement Potential

In order to obtain some ground to the above explanation, one consider the confinement potential which can be obtained starting from a Coulomb-like potential responsible by the strong interaction in short distance and a linear part describing the nature of confinement. Thus the confinement potential in the lowest order can be written as follows [35]:

$$V_c(\mu, r) = -4\alpha_s(\mu)/3r + \kappa r, \quad (18)$$

where r is now the spatial separation for pair, strictly speaking, infinitely heavy (static) quark and antiquark inside the hadron, $\alpha_s(\mu)$ is the running coupling constant of the strong interaction at a specific energy scale μ [34] and κ is called string tension which in general depends on temperature and characterizes the average estimation $\sqrt{\kappa} \approx 0.405$ GeV [36] for cold strongly interacting matter. The exact analytic view of the $\alpha_s(\mu)$ within 1-loop approximation is

$$\alpha_s(\mu) = (\beta_0 t)^{-1}, \quad (19)$$

where $t \equiv \ln(\mu^2/\Lambda_{\text{QCD}}^2)$, $\beta_0 = (33 - 2n_f)/12\pi$ is the 1-loop β -function coefficient, n_f is the number of quark flavors active at the energy scale μ , i.e. are considered light $m_q \ll \mu$, m_q is the quark mass, Λ_{QCD} is non-universal scale parameter depending on the renormalization scheme adopted and corresponds to the scale where the perturbatively-defined coupling would diverge [34]. The numerical value of the Λ_{QCD} depends, in particular, on n_f and here the certain value Λ_{QCD} from [34] is used for given n_f . At present the convenient estimation of the $\alpha_s(\mu)$ is calculated to complete 4-loop approximation [34, 37]. Moreover, the running coupling constant can be defined from any physical

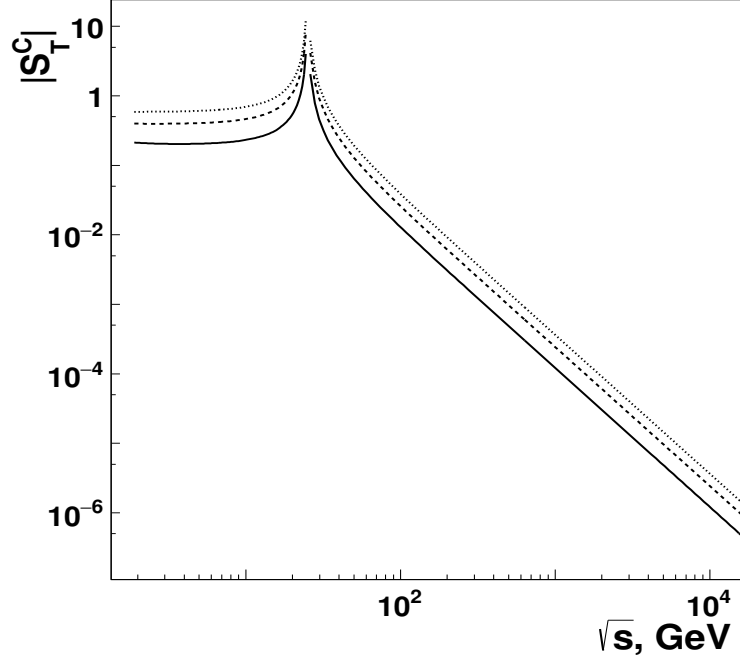


FIG. 3: Absolute values of the TE deduced for Coulomb potential in the impact parameter space on collisions energy considering $\sqrt{s_c} = 25.0$ GeV, $b_{\min} = \sqrt{6/s_{l.b.}}$ and $b_{\max} = 10b_{\min}$. The solid curves correspond to the $b = 0.5$ fm, dashed one – to the $b = 1.0$ fm and dotted lines are for $b = 1.5$ fm. More details are described in the text.

observable perturbatively calculated [38] and to each μ one obtains a α_s resulting in specific (18). As seen from (19) one must require $\mu > \mu_{\min} \equiv \omega \Lambda_{\text{QCD}}$ in order to preserve the validity of the perturbative definition of the coupling $\alpha_s(\mu)$. The softest case corresponds to the $\omega = 1$ and more conservative and exact estimation is the following [38]:

$$\omega = \exp[F_0(\alpha_s^{\max})/2\beta_0], \quad (20)$$

where $\alpha_s^{\max} = \beta_0/\beta_1$, $F_0(x) = x^{-1} + \beta_1/\beta_0 \ln(\beta_0 x)$, $\beta_1 = (153 - 9n_f)/24\pi^2$ is the 2-loop β -function coefficient [34].

There are several ways for estimation of the μ based on the experimentally measurable quantity Y_h^{exp} in hadronic collisions, for instance, it is assumed $\mu = Y_h^{\text{exp}}$ at $Y_h^{\text{exp}} \equiv p_T^{\max}$ [39] or $Y_h^{\text{exp}} \equiv m_3$ [40] in some recent studies, where p_T^{\max} is the transverse momentum of the leading jet, m_3 is the invariant mass of the three jets leading in p_T . In particular, the energy scale μ may be connected to the s by assuming the simple relation $\mu^2 = \eta s$ where $0 < \eta \leq 1$ which implies that μ is just a fraction of the energy involved in the elastic scattering process². This assumption is analogous momentum fraction x carried by a scattered quark in deep inelastic scattering (DIS). Taking into account the energy balance in collisions of the finite-size particles one can put $\eta = 1/9$ [41]. As proposed in [13], the hadron density grows as the energy increases by a change in the fractal dimension of the total cross section. It can be viewed as an increase in the parton density which means very small values of x . The cutoff in the parton density growth is studied by the Balitski–Kovchegov equation which realizes this saturation through pomeron fan diagrams [42]. On the other hand, as the density grows, the distances diminish between constituents (q and \bar{q}) in the pair and between pairs itself. The confinement potential is of short-range in contrast with the Coulomb one and due to uncertainty principle the quantity μ_{\min} allows the unambiguous estimation the linear scale $r_{\max} \sim \mu_{\min}^{-1}$ up to which the confinement potential can be calculated with help of the (18). One can expect $r_{\max} \sim R_h$ depending on the approach to μ_{\min} and values of the Λ_{QCD} at given n_f [34], where R_h is the hadron radius. This upper cutoff for r leads to tame the divergence of the confinement potential (18). In general, it should be $b \leq b_{\max} \sim r_{\max}$ in order to the incoming particles interact by strong force with each other, on the other hand smaller space scale $r \rightarrow 0$ into hadron can be probed in more central collisions with $b \rightarrow 0$. Therefore one can assume $r = \varepsilon_2 b$, where $\varepsilon_2 \leq 1$ and the confinement

² One can note that $\eta = 1$ within the approach of point-like particles used above in the Sec. III A which corresponds to the case of interactions between structureless fundamental constituents (fermions, bosons) of the Standard Model (SM) at present accuracy level.

potential in the impact parameter space can be rewritten as

$$V_c(\mu, r) = V_c(s, b) = -4\alpha_s(\eta s)/3\varepsilon_2 b + \kappa\varepsilon_2 b. \quad (21)$$

In contrast with the Coulomb potential the $V_c(\mu, r)$ and $V_c(s, b)$ coincide exactly in whole domain ($\mu \geq \mu_{\min}; r \leq r_{\max}$) due to exact (linear) interrelations between corresponding terms in the parameter pairs (μ, r) and (s, b) . Taking into account the general properties of hadronic collisions discussed above, it is used $\varepsilon_2 = 1.0$ for the sake of simplicity, unless otherwise specifically indicated.

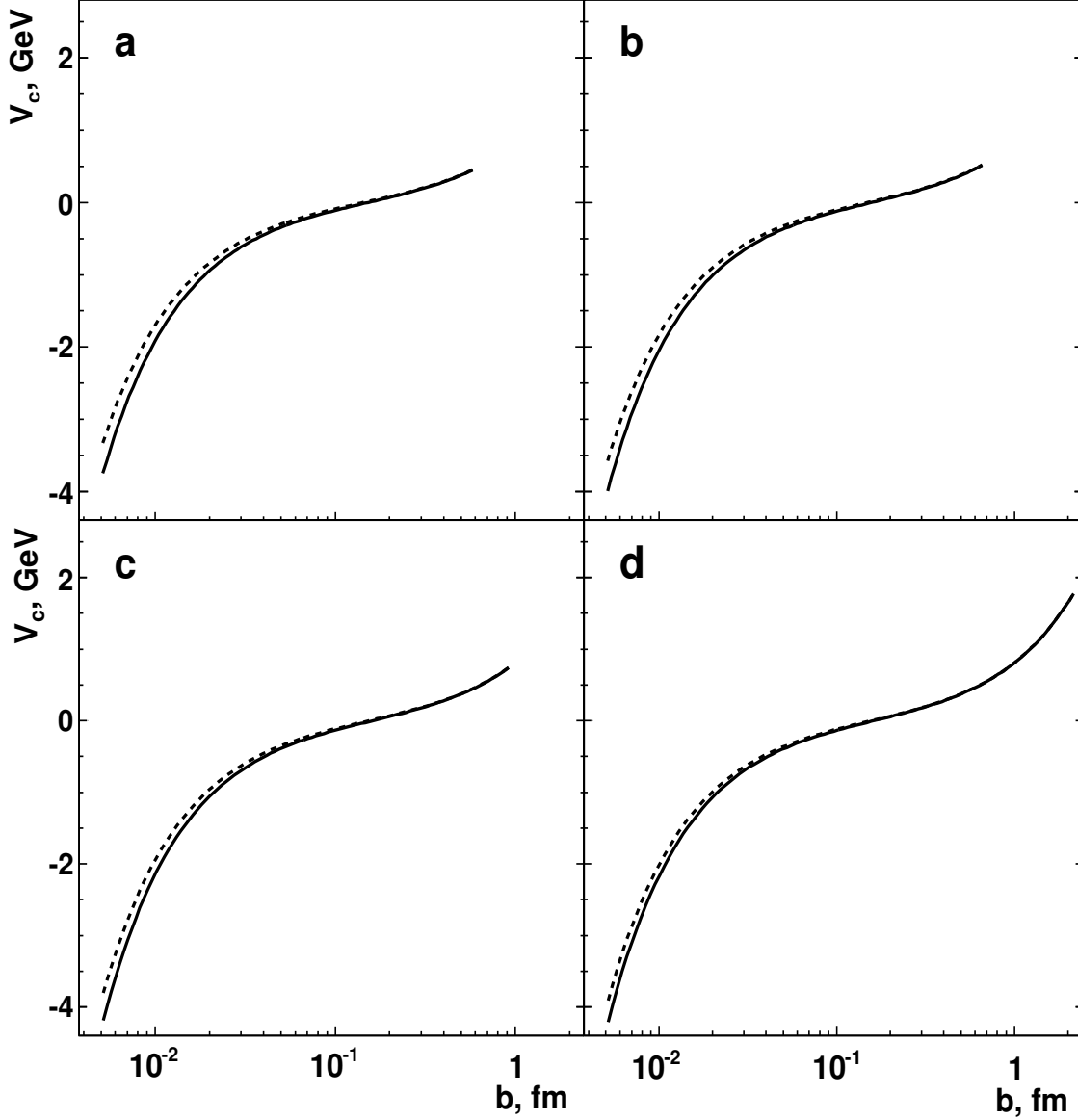


FIG. 4: Dependence of the confinement potential on impact parameter at $\sqrt{s} = 14$ TeV and $n_f = 3$ (a), $n_f = 4$ (b), $n_f = 5$ (c) and $n_f = 6$ (d) with various approximations for $\alpha_s(\mu)$: solid line is for the 1-loop solution (19) and dashed curve corresponds to the 4-loop approximation [34]. The softest scheme for μ_{\min} is used without loss of generality.

Contrary to the Coulomb potential, the confinement potential allows a first glance at the hadron internal arrangement revealing its importance to the correct description of the scattering. Fig. 4 shows the b -dependence of the

confinement potential (21) at fixed $\sqrt{s} = 14$ TeV and various numbers of the light flavors³ n_f for 1- and 4-loop approximation for $\alpha_s(\mu)$. The value $\omega = 1$ is used for definition of the μ_{\min} and, consequently, the largest value of the upper cutoff for b . The 4-loop approximation for $\alpha_s(\mu)$ provides slightly larger values of $V_c(s, b)$ than that for 1-loop exact solution (19) in the range of small values $b \lesssim 0.03$ fm only and the consistent transition from Fig. 4a to Fig. 4d demonstrates the weakening difference between the two curves with growth of n_f . Thus in general the order of approximation for $\alpha_s(\mu)$ influences weakly on the $V_c(s, b)$ in whole range of the b at any n_f under consideration and results below are robust with respect to the scheme for calculation of the $\alpha_s(\mu)$. For definiteness the modern 4-loop approximation is used for $\alpha_s(\mu)$ below, unless otherwise specifically indicated. At intermediate energy $\sqrt{s} = 52.8$ GeV the view $V_c(s, b)$ does not depend on the number of light flavors (Figs. 5a, b). The dependence of the confinement potential on n_f manifests itself in the high energy domain only, for instance at $\sqrt{s} = 14$ TeV, in which the wide set of the values of n_f is available (Figs. 5c, d). In the last case the growth of n_f has provided some decrease of the $V_c(s, b)$ at small $b \lesssim 0.03$ fm and expected, expanding of the confinement potential to the larger impact parameter values $b \gtrsim R_h$ due to the decrease of Λ_{QCD} . The changing of the scheme for estimation of the μ_{\min} does not influence on the functional behavior of the $V_c(s, b)$ for both the intermediate (Figs. 5a, b) and the high energy (Figs. 5c, d) under study. The transition from the $\omega = 1$ (Figs. 5a, c) to the conservative estimation of this parameter (Figs. 5b, d) leads to the decrease of the high boundaries for linear scales r and b . Fig. 6 shows the evolution of the $V_c(s, b)$ with collision energy growth at fixed $n_f = 3$ (a, b) and $n_f = 4$ (c, d) for two different approaches for μ_{\min} . As seen the $V_c(s, b)$ larger for $\sqrt{s} = 14$ TeV than that for $\sqrt{s} = 52.8$ GeV at corresponding values of b for any number of light flavors n_f and scheme for the ω -parameter calculation. Furthermore, the difference between two curves increases with decreasing of b . The behavior of the $V_c(s, b)$ in Fig. 6 is explained by the smooth decreasing of $\alpha_s(\mu)$ with growth of μ [34], i.e. with collision energy due to the relation used in the paper.

In general the main features of the confinement potential shown in Figs. 4 – 6 are driven by contributions of the different terms in (18) or, consequently, (21) for various ranges of the values of impact parameter. The $V_c(s, b)$ is sensitive to the changing of n_f , s mostly at small b because the main contribution in this range comes from the first (short-range) term in (21) containing $\alpha_s(\mu)$ that depends, in turn, on n_f and s . The influence of the first term decreases with the growth of the b and contribution of the second (long-range) term becomes dominant in (21). This term depends on string tension only and, consequently, $V_c(s, b)$ does not sensitive for n_f and changes much weaker with s for relatively large $b > 0.1$ fm.

It is necessary to normalize the potential (21) in order to obey the unitarity condition. As it is well known the second term in (18) and (21) provides the main difference of the confinement potential from the Coulomb one, namely, the positive values and quasi-linear growth of the $V_c(s, b)$ at large b , i.e. r (Figs. 4 – 6). The confinement potential passes through the zero value at

$$b_0 = \varepsilon_2^{-1} \sqrt{\zeta} \propto \sqrt{\alpha_s(\eta s)}, \quad \zeta \equiv 4\alpha_s(\eta s)/3\kappa, \quad (22)$$

where the allowable ranges are taken into account for linear scales r and b , i.e. $r, b > 0$. One can use the (15) with appropriate values of m if the confinement potential has constant sign within b -range under consideration. But in general potential $V(s, b)$ may change the sign within the kinematic domain under study and this feature can lead to the discontinuity for $\tilde{V}(s, b)$ if extremum (maximum) value of the $V(s, b)$ is used as the scale factor. Analysis shows that the using of the maximum for the absolute value of the potential, $|V(s, b)|_{\max}$, avoids possible discontinuity in the behavior of the $\tilde{V}(s, b)$ in the case of changing the sign of $V(s, b)$. Therefore here the following relation is used

$$\tilde{V}_c(s, b) = |V_c(s, b)|/|V_c(s, b)|_{\max}. \quad (23)$$

where $|V_c(s, b)|$ is the absolute value of the confinement potential $V_c(s, b)$ if the confinement potential changes the sign within b -range under discussion. In this case the $|V_c(s, b)|_{\max}$ can be reached at low or right boundary of b (Figs. 4 – 6). Without lost of generality the range $b_{\min} \leq b \leq b_{\max}$ is studied below, where $V_c(s, b_{\min}) < 0$ and b_{\max} is driven by the r_{\max} . Thus the normalized confinement potential in the impact parameter space can be written as follows:

$$\tilde{V}_c(s, b) = \begin{cases} \frac{b}{b_{\min}} \left| \frac{1 - \zeta/(\varepsilon_2 b)^2}{1 - \zeta/(\varepsilon_2 b_{\min})^2} \right|, & \text{if } |V_c(s, b_{\min})| > V_c(s, b_{\max}); \\ \frac{b}{b_{\max}} \left| \frac{1 - \zeta/(\varepsilon_2 b)^2}{1 - \zeta/(\varepsilon_2 b_{\max})^2} \right|, & \text{if } |V_c(s, b)|_{\max} = V_c(s, b_{\max}). \end{cases} \quad (24)$$

³ The condition $\mu \geq \varepsilon_3 m_q$ is used for definition of the quark with certain flavor as light one for calculations within the present paper at $\varepsilon_3 = 10$.

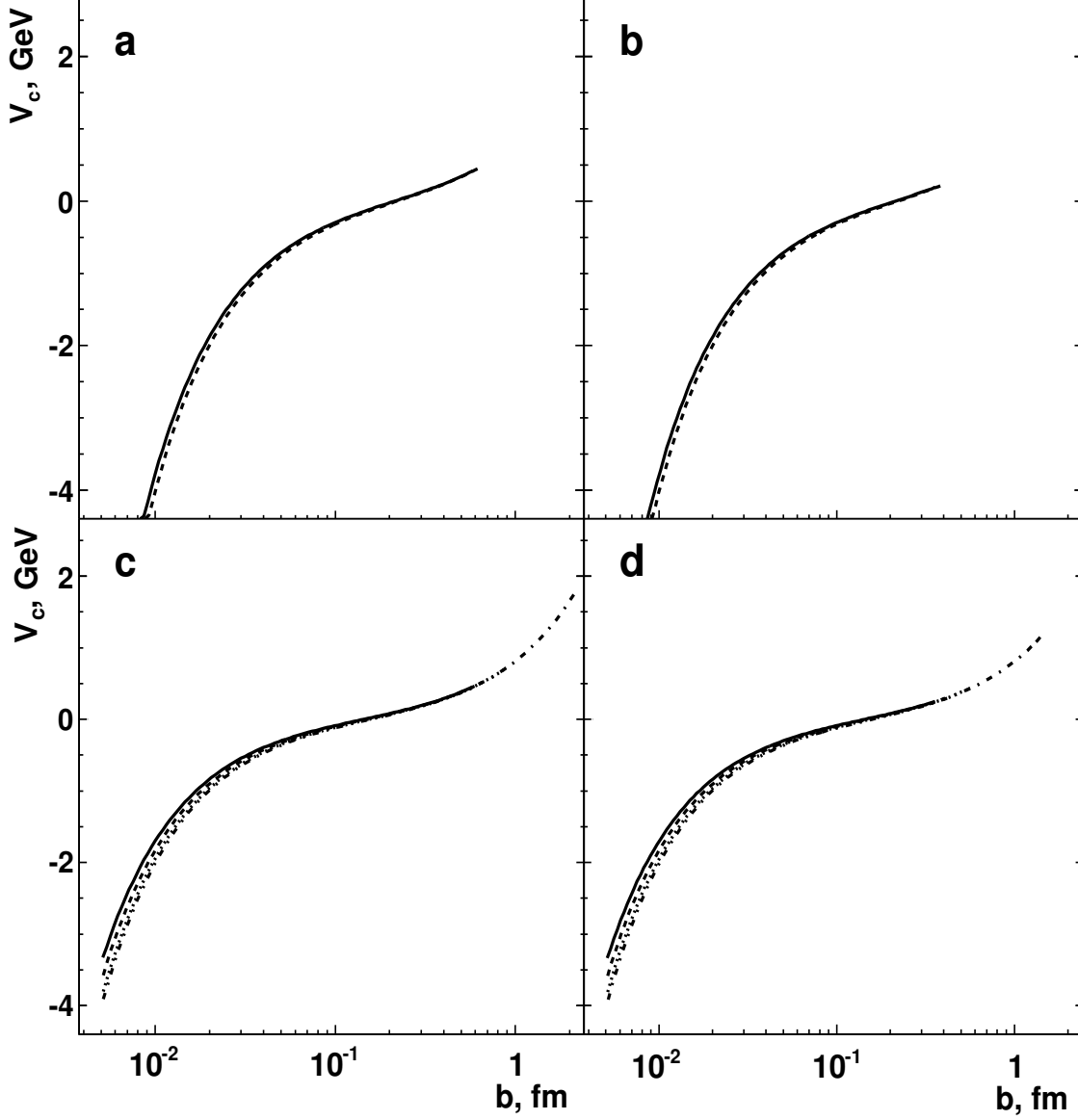


FIG. 5: Dependence of the confinement potential on impact parameter at $\sqrt{s} = 52.8$ GeV (a, b) and $\sqrt{s} = 14$ TeV (c, d) for various n_f : solid line is for $n_f = 3$, dashed one – for $n_f = 4$, dotted curve corresponds to the $n_f = 5$ and dot-dashed one – to the $n_f = 6$. The left column (a, c) shows results for $\omega = 1$ and curves for conservative estimation (20) are in the right column (b, d).

Here it is assumed that the confinement potential is still characterized by finite negative value for the value b_{\min} of impact parameter⁴. As seen $V_c(s, b_{\max}) < 2$ GeV for any loop approximation (Fig. 4), scheme for μ_{\min} estimation and n_f values (Fig. 5), as consequence, the condition $|V_c(s, b)|_{\max} = V_c(s, b_{\max})$ is valid until to $b_{\min} \gtrsim 10^{-2}$ fm. Therefore the lower relation in (24) is mostly applicable, the upper equation in (24) is only for processes which probe the inner structure of a hadron down to the very small linear scales. The qualitative conclusions follow from relations (24) in the domain of validity of the condition $\zeta \ll (\varepsilon_2 b)^2$. Here the normalized confinement potential and corresponding

⁴ One can note that there is no limit of the b_{\min} because it can be $\mu \rightarrow \infty$ in general. The present experimental restriction on the size of fundamental constituents of the SM can be suggested as the estimation of the low boundary ($b_{l.b.}$) of the b_{\min} in the relation (24): $b_{\min} \geq b_{l.b.} \sim 2 \times 10^{-4}$ fm at $\mu_{\max} \sim 1$ TeV [34].

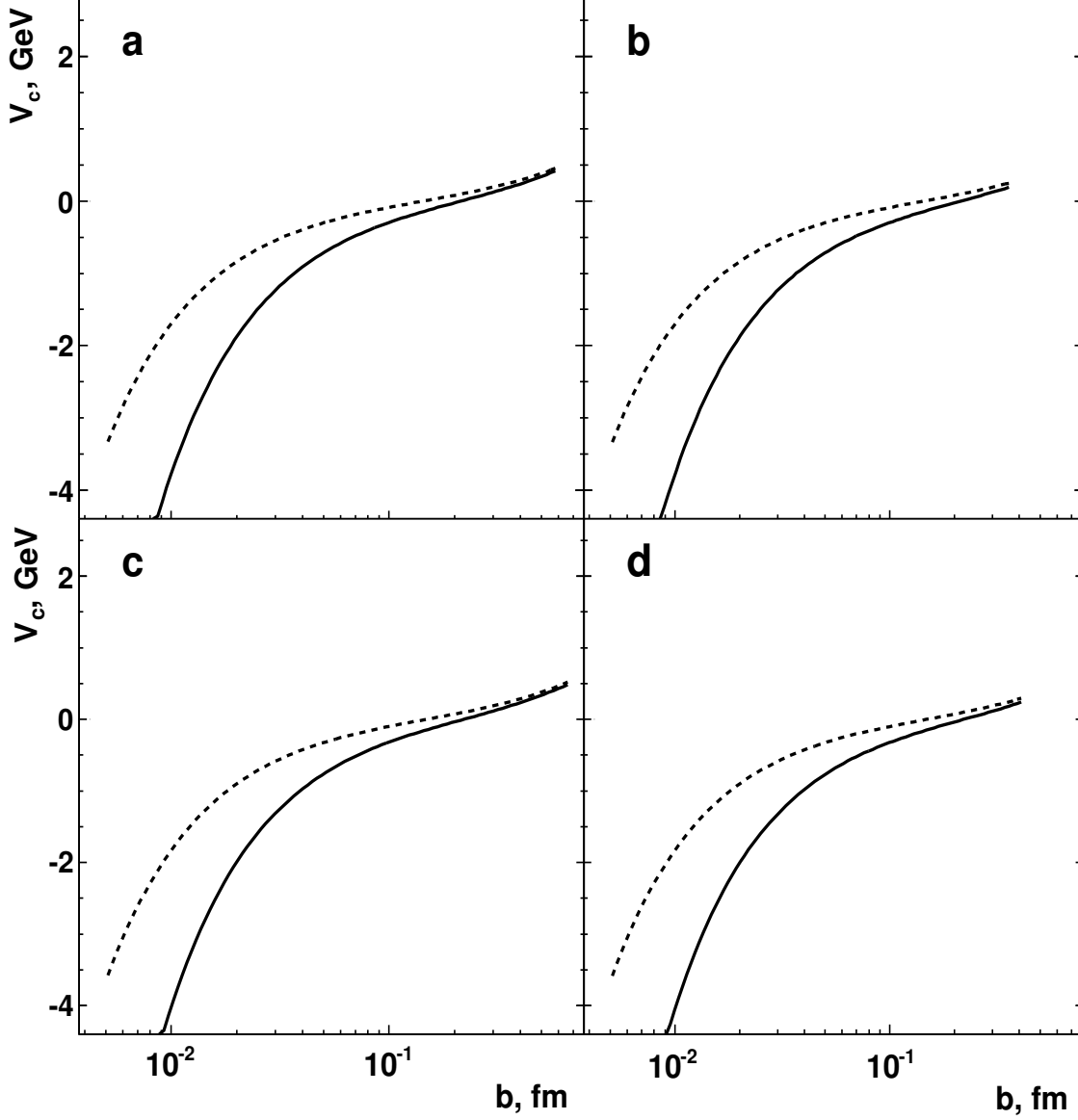


FIG. 6: Dependence of the confinement potential on impact parameter at $n_f = 3$ (a, b) and $n_f = 4$ (c, d) for two collision energies: solid line is for $\sqrt{s} = 52.8$ GeV and dashed one – for $\sqrt{s} = 14$ TeV. The left column (a, c) shows results for $\omega = 1$ and curves for conservative estimation (20) are in the right column (b, d).

inelastic overlap function $G_{\text{inel}}^c(s, b)$ are weakly sensitive on changing of the n_f and s , the energy dependence of the TE S_T^c is driven by the k .

Fig. 7 shows the dependence of the inelastic overlap function for confinement potential $G_{\text{inel}}^c(s, b)$ on b at various n_f and approaches for ω for two collision energies $\sqrt{s} = 52.8$ GeV (a, b) and 14 TeV (c, d). The certain scheme for ω estimation does not influence on the $G_{\text{inel}}^c(s, b)$ at intermediate energy (Fig. 7a, b) but the situation is another at $\sqrt{s} = 14$ TeV (Fig. 7c, d): the conservative estimation for ω leads to smaller $G_{\text{inel}}^c(s, b)$ at $b < b_0$ in comparison with the case for $\omega = 1$ and the influence is weaker for larger n_f . The influence of the n_f on the view of $G_{\text{inel}}^c(s, b)$ is negligible at $\sqrt{s} = 52.8$ GeV (Fig. 7a, b) and the growth of the number of light flavors leads to the increase in $G_{\text{inel}}^c(s, b)$ at fixed b for $\sqrt{s} = 14$ TeV (Fig. 7c, d) especially for large $n_f = 5$ and 6. For the confinement potential the regime of black disk $G_{\text{inel}}^c(s, b) \approx 1$ is reached at b_0 and in the region close to this inflection point of the $V_c(s, b)$ and, as discussed above, the region expands with the growth of the n_f especially for largest $n_f = 6$. Such behavior agrees with qualitative expectation for expansion of the region with high absorption in the nucleon-nucleon collisions at higher energies. On the other hand the general feature of the $G_{\text{inel}}^c(s, b)$ in Fig. 7 is the more transparent (gray)

regions at both the small ($b \ll b_0$) and the large ($b \gg b_0$) impact parameters. Therefore the confinement potential provides the hollowness effect on central collisions at high energy $\sqrt{s} = 14$ TeV (Fig. 7c, d). In general the behavior of $G_{\text{inel}}^c(s, b)$ in Fig. 7 obtained within potential approach confirms the results from [2, 3] and the analyzes done by [4–11]. Furthermore one expects that inelastic overlap function description is better to small b values considered.

Fig. 8 demonstrates $G_{\text{inel}}^c(s, b)$ in dependence on b at various \sqrt{s} and approaches for ω for two different numbers of light flavors $n_f = 3$ (a, b) and 4 (c, d). The various behaviors of $G_{\text{inel}}^c(s, b)$ at $\sqrt{s} = 14$ TeV in dependence of the scheme for estimation of ω leads to the different relations between inelastic two overlap functions at $n_f = 3$ in Figs. 8a and 8b, at $n_f = 4$ in Figs. 8c and 8d. The maximum of $G_{\text{inel}}^c(s, b)$ goes to the smaller $b \simeq 0.15$ fm with the increase of \sqrt{s} . At $\omega = 1$ the $G_{\text{inel}}^c(s, b)$ is significantly larger at $\sqrt{s} = 14$ TeV than that for $\sqrt{s} = 52.8$ GeV at $b \lesssim 0.15$ fm and vice versa at larger $b \gtrsim 0.3$ fm for both the $n_f = 3$ (Fig. 8a) and the $n_f = 4$ (Fig. 8c). Thus the region of stronger absorption shifts to the smaller b , i.e., appear in more central collisions, at $\sqrt{s} = 14$ TeV with regard of the corresponding region at intermediate energy $\sqrt{s} = 52.8$ GeV. At conservative estimation (20) the behavior of the maximum of $G_{\text{inel}}^c(s, b)$ is the same in dependence of the \sqrt{s} but the excess of the inelastic overlap function at $\sqrt{s} = 14$ TeV over the quantity at $\sqrt{s} = 52.8$ GeV is seen in significantly narrower region $0.07 \lesssim b \lesssim 0.15$ fm with opposite relation between these overlap functions at larger b and the close behavior of $G_{\text{inel}}^c(s, b)|_{\sqrt{s}=52.8 \text{ GeV}}$ and $G_{\text{inel}}^c(s, b)|_{\sqrt{s}=14 \text{ TeV}}$ at smaller b . These statements are valid at $n_f = 3$ (Fig. 8b) and $n_f = 4$ (Fig. 8). Thus the conservative scheme for ω lead to the hollowness effect at the close b for both very difference energies under consideration.

In Figs. 7, 8 all curves reveal the presence of a critical value b_0 according the analyzes performed in the preceding section showing the existence of a gray area at $b < b_0$. Although the use of confinement potential is a naive approach, it is interesting to note that the description of the inelastic overlap function shows the black disk limit occurring to $b \neq 0$ and a clear gray area (the hollowness effect) near $b = 0$.

It should be stressed that the Λ_{QCD} is estimated for $n_f \geq 3$ only [34]. Thus one can consider $\mu \geq 0.96$ GeV, i.e. $\sqrt{s} \geq 2.88$ GeV based on the perturbatively-defined coupling for strong interactions and with taking into account the condition for the lightness of the quark with certain flavor as well as the relation between μ^2 and s above. This energy range cover almost all energies allowed for nucleon-nucleon collisions with exception of the narrow region close to the low boundary $\sqrt{s_{\text{l.b.}}}$.

The characteristic linear scales in the impact parameter space – b_{min} , b_0 and b_{max} – depend on s . Also the dependence on the number of loops for approximation of the $\alpha_s(\eta s)$ is for b_0 , there is dependence on the scheme for the estimation μ_{min} for the b_{max} . Within the general framework of the paper the relation $b_{\text{min}} \sim \mu^{-1} = (\eta s)^{-1}$ is used for rough estimation of the lower boundary for impact parameter in collisions with given s . The 1-loop approximation for $\alpha_s(\eta s)$ provides some larger b_0 than 4-loop approximation at low and intermediate energies. The relative excess is less than 0.2 at the lowest energy $\sqrt{s} = 2.88$ GeV, it decreases with increasing s and difference between values of b_0 obtained within two various loop approximations are negligible at $\sqrt{s} \gtrsim 200$ GeV. Values of b_0 are in the range from on about 0.40–0.50 fm at the lowest allowed s down to the $\simeq 0.17$ fm at $\sqrt{s} = 14$ TeV. The detailed analysis of the dependence $b_{\text{max}}(s)$ shows that the b_{max} is constant at fixed n_f and increases changes sharply within narrow range of s as the new flavor begins to be sufficient. The magnitude of the step increases consequently with onset of influence of heavier flavors and quantity is largest for transition from $n_f = 5$ to $n_f = 6$. As expected the difference is constant between values of b_{max} obtained with help of $\omega = 1$ and ω defined by (20) at given n_f . Values of b_{max} are in the range from on about 0.60 (0.35) fm at $\sqrt{s} = 2.88$ GeV to the $\simeq 2.20$ (1.50) fm at the nominal LHC energy $\sqrt{s} = 14$ TeV for the softest (conservative) restriction on the μ_{min} . It is interesting to note that $b_0 \gtrsim b_{\text{max}}$ at $\sqrt{s} \approx 2.88$ GeV for ω defined by (20) and 4-loop approximation, i.e. in this case $\forall b : V_c(s, b) < 0$ in the very narrow energy range close to the lowest allowed value of s .

The b -dependence of the TE for confinement potential (S_T^c) is driven by the Figs. 7, 8 and relation (16).

As for the Coulomb potential the sign of the S_T^c is defined by the k due to normalization procedure and the TE for confinement potential is characterized by sharp changing near s_c . The absolute values of the TE for $s < s_c$ ($|S_T^c| = -S_T^c$) are larger by orders than that for $s > s_c$ ($|S_T^c| = S_T^c$). Therefore, as well as in Subsec. III A the $|S_T^c|$ is the adequate quantity for study of s -dependence of the TE for the approximation (21) of the confinement potential in b -space. Fig. 9 shows the energy behavior of absolute value of the TE for confinement potential within 4-loop approximation for α_s at $b_{\text{min}} = 0.05$ fm, $\sqrt{s_c} = 25.0$ GeV, softest (a) and conservative (b) restriction on the μ_{min} for various b . Additional analysis shows that $|S_T^c|(s, b)$ does not depend on the scheme for estimation of the ω at given value of impact parameter⁵. Thus the values of b differ in Fig. 9a and 9b for most cases. As expected the k provides the similar general trends for the energy dependence of the TE in Fig. 9 in comparison with the Fig. 3. But the behavior of $|S_T^c(s, b)|$ is more complex than that for Coulomb potential. The very sharp minimums are the

⁵ See, for instance, the curves at $b = 0.10$ fm in Fig. 9a and 9b.

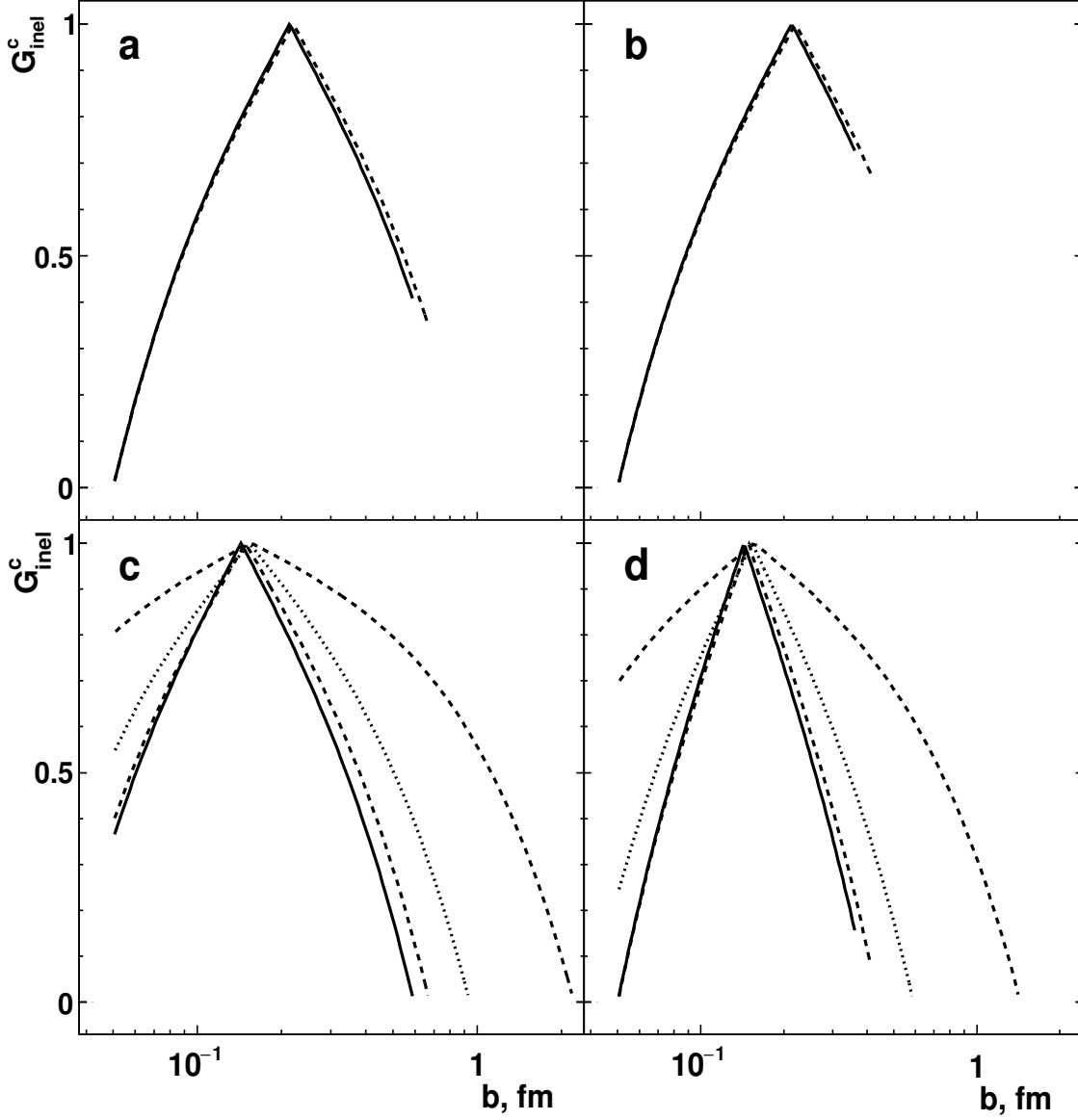


FIG. 7: Behavior of $G_{\text{inel}}^c(s, b)$ using the confinement potential at $b_{\text{min}} = 0.05$ fm, $\sqrt{s} = 52.8$ GeV (a, b) and $\sqrt{s} = 14$ TeV (c, d) for various n_f : solid line is for $n_f = 3$, dashed one – for $n_f = 4$, dotted curve corresponds to the $n_f = 5$ and dot-dashed one – to the $n_f = 6$. The left column (a, c) shows results for $\omega = 1$ and curves for conservative estimation (20) are in the right column (b, d).

$|S_T^c(s, b)| = 0$ at \sqrt{s} for which $b = b_0$. As discussed above the sharp changing of the $|S_T^c(s, b)|$ due to onset of influence of heavier flavors is most visible for $n_f = 6$ in TeV-energy range.

IV. DISCUSSIONS AND CONCLUSIONS

The presence of the hollowness effect (gray area) cannot be associated with the limiting resolution of the facilities. Of course, the de Broglie wavelength achieves its minimum at present day energies at CERN LHC, but besides its small value $\Delta r = 1/p_{cm} \sim 2/\sqrt{s}$ it still produces an unavoidable natural coarse-grain effect.

The entropy is probably the most important physical quantity of nature and should be taken into account in all explanations of basic physics. Here, the entropy is used in its Tsallis form. The entropic index- w represents a phase transition occurring at $s = s_c$ in total cross section picture. The probability density function is replaced by the

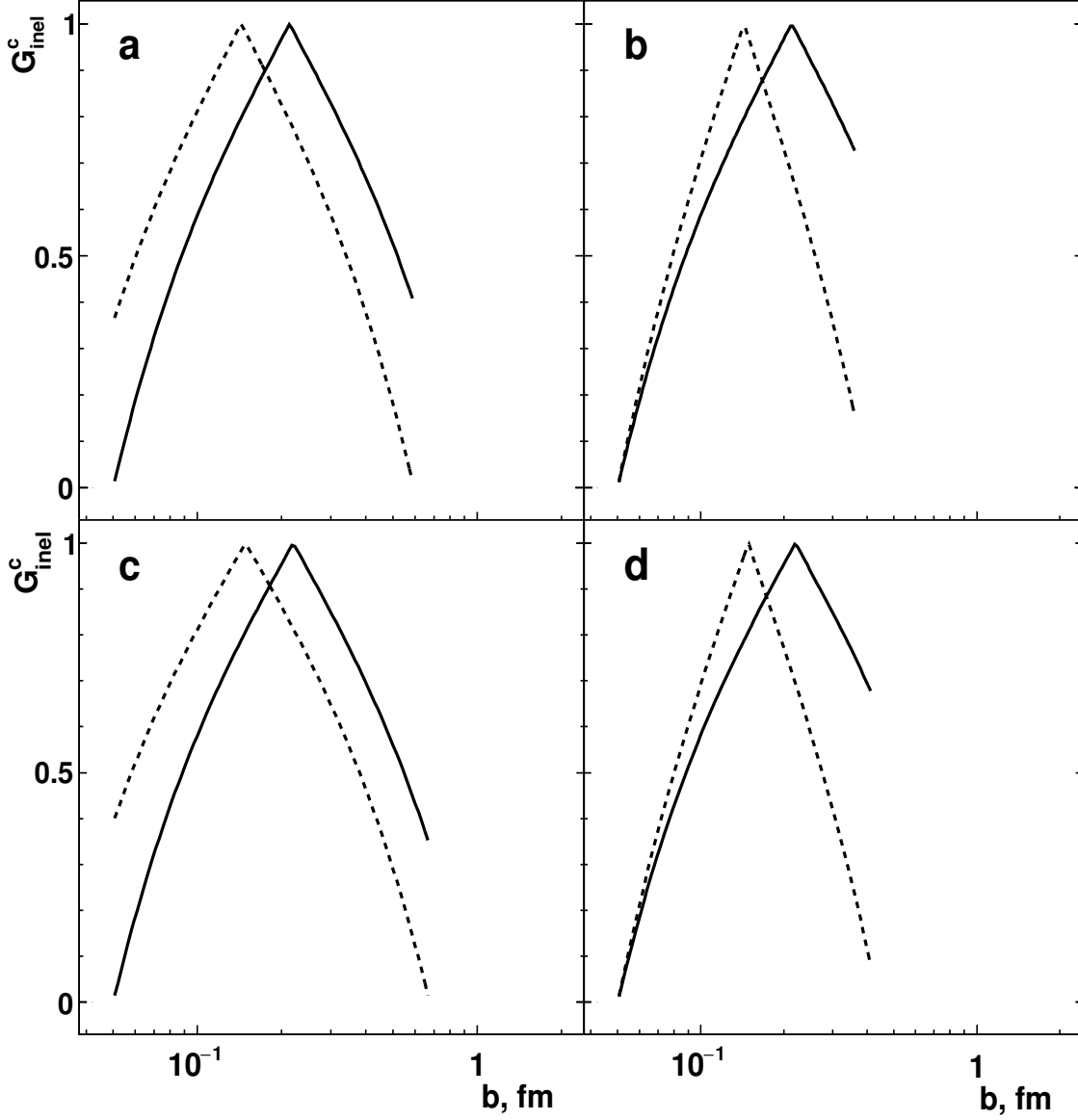


FIG. 8: Behavior of $G_{\text{inel}}^c(s, b)$ using the confinement potential at $b_{\text{min}} = 0.05$ fm, $n_f = 3$ (a, b) and $n_f = 4$ (c, d) for two collision energies: solid line is for $\sqrt{s} = 52.8$ GeV and dashed one – for $\sqrt{s} = 14$ TeV. The left column (a, c) shows results for $\omega = 1$ and curves for conservative estimation (20) are in the right column (b, d).

inelastic overlap function of the impact parameter space. Therefore, this form of entropy can allow the understanding of how the matter density induces the geometrical pattern observed.

The TE is one of several one ways to compute the entropy of a non-additive system. However, without loss of generality, the cases of interest can be reduced to the Tsallis form, even the additive entropies by taking $w = 1$ [30, 31].

The increasing or decreasing entropy implies in an increasing or decreasing probability of the inelastic overlap function which result is the emergence of a critical value b_0 to the distribution of matter inside pp and $\bar{p}p$ elastic scattering. Therefore, the entropy determines the existence of a critical value in the impact parameter space. The consequence of that can be viewed as the presence of a fractal character in the transferred momentum space [15–20].

The behavior of $\partial_b G_{\text{inel}}(s, b)$ is analyzed by assuming two considerations: by analyzing $\text{Re}\Gamma(s, b)$ and $\partial_b \tilde{S}$. The first one is connected to the $\text{Im}F(s, b)$ and the second to the thermodynamic properties of the TE. In both situations the result of the behavior is the same. Of course, one cannot prove the uniqueness of the behavior of $G_{\text{inel}}(s, b)$ presented in Figs. 7, 8 since there are subtle choices of parameters where $\partial_b \tilde{S}$ does not present that behavior. However, based

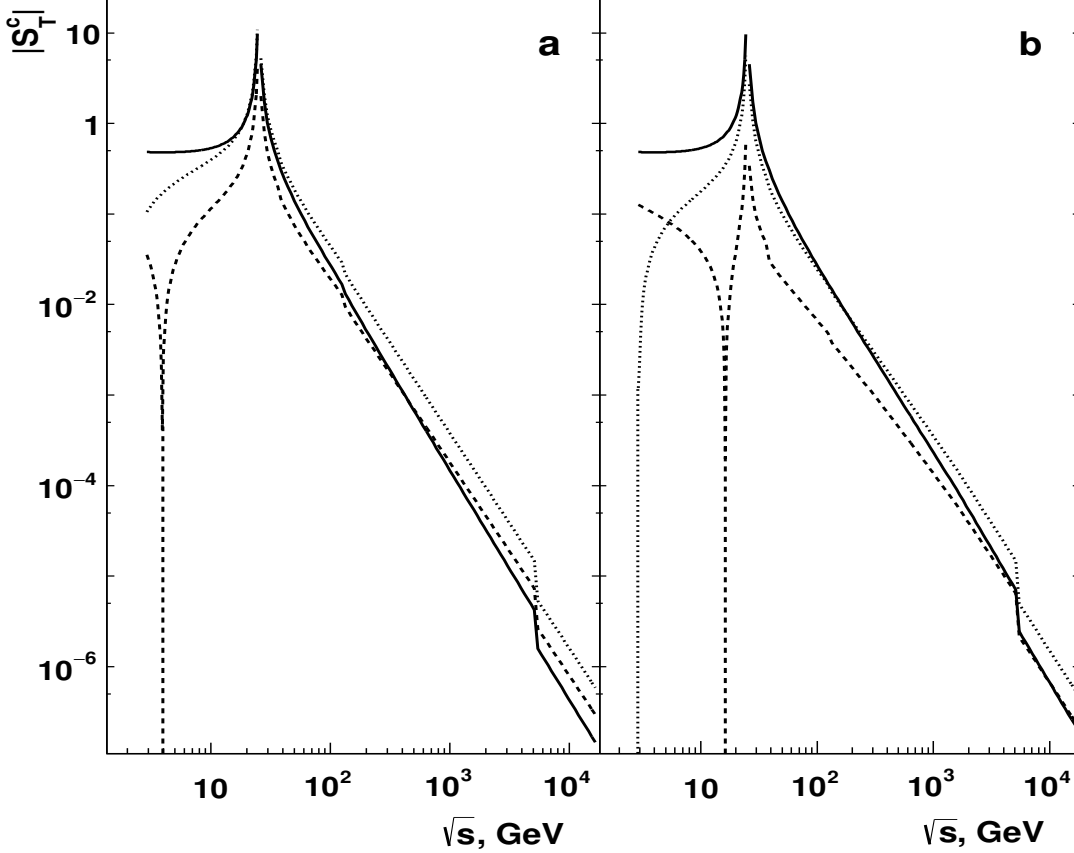


FIG. 9: Absolute values of the TE deduced for confinement potential in the impact parameter space on collisions energy considering $b_{\min} = 0.05$ fm, $\sqrt{s_c} = 25.0$ GeV, softest (a) and conservative (b) restriction on the μ_{\min} . The solid lines are for $b = 0.10$ fm while dashed curve corresponds to the $b = 0.35$ fm in (a) and $b = 0.25$ fm in (b), dotted lines are for $b = 0.60$ fm (a) and 0.40 fm (b).

on the $\partial_b \text{Re}\Gamma(s, b)$ it seems to be unlikely.

The use of potentials to mimic the internal energy is not new to physics, probably remounting to Bohm quantum potential [43] in Quantum Mechanics and more recently to [32] in nuclear scattering. However, the use here of the Coulomb and the confinement potentials are illustrative of the physical behavior of pp and $\bar{p}pp$ in the impact parameter space.

The Coulomb potential treats the hadrons as point-like objects and its description using the impact parameter picture does not allow any consideration near forward direction. Far from the forward direction (high q^2), derivative terms can be added in order to achieve a better description of the inelastic overlap function introducing a slow down decaying to the tail.

On the other hand, the confinement potential considered here as the internal energy of the hadron shows the hollowness effect. Derivative terms can be taken into account in order to obtain a better description of the tail of the inelastic overlap function (low q^2). However, these terms does not interfere in the description near forward collisions. Therefore, the confinement potential allows the emergence of this effect even if we add derivative terms.

In order to avoid the hollowness effect (from the point of view of the confinement) we should modify the confinement potential by adding correction terms which acts only near forward direction. These terms can, for instance, to correspond to the kinematic terms emerging at very high q^2 (very short distances). However, it seems unlikely since corrections to the linear term of (21) implies or in the decreasing of the strength of the confinement potential to $b \rightarrow 0$ or simply by not modifying its general behavior to $b \rightarrow 0$ (or introducing some noise or small perturbations). None of these assumptions seem to be physically reasonable. Therefore, we claim here that the presence of a gray area in the impact parameter space reflects the multifractal character of the hadron in the energy and momentum spaces.

The analyzes carried out here are based on few physical assumptions and allows one to obtain the occurrence of the gray area in the inelastic overlap function without the use of models on pp and $\bar{p}p$ elastic scattering. Furthermore,

the results obtained here can help in the construction of models taking into account the existence of the gray area and the entropy of the collision process.

Acknowledgments

S.D.C. thanks to UFSCar by the financial support. The work of V.A.O. was supported partly by NRNU MEPhI Academic Excellence Project (contract No 02.a03.21.0005, 27.08.2013).

-
- [1] F. Zimmermann, EuCARD-REP-2013-009 (2014).
 - [2] I.M. Dremin, Phys. Uspekhi **58**, 61 (2015).
 - [3] I.M. Dremin, Phys. Uspekhi **60**, 333 (2017).
 - [4] W. Broniowski and E. Ruiz Arriola, Acta Phys. Polon. B Proc. Supp. **10**, 1203 (2017).
 - [5] A. Alkin, E. Martinov, O. Kovalenko and S.M. Troshin, Phys. Rev. D **89**, 091501 (2014).
 - [6] V.V. Anisovich, V.A. Nikonov and J. Nyiri, Phys. Rev. D **90**, 074005 (2014).
 - [7] S.M. Troshin and N.E. Tyurin, Int. J. Mod. Phys. A **29**, 1450151 (2014).
 - [8] V.V. Anisovich, Phys. Uspekhi **58**, 1043 (2015).
 - [9] S.M. Troshin and N.E. Tyurin, Mod. Phys. Lett. A **31**, 1650079 (2016).
 - [10] J.L. Albacete and A. Soto-Ontoso, Phys. Lett. B **770**, 149 (2017).
 - [11] E. Ruiz Arriola and W. Broniowski, Phys. Rev. D **95**, 074030 (2017).
 - [12] S.D. Campos, V.A. Okorokov and C.V. Moraes, *in preparation*.
 - [13] F.S. Borcsik and S.D. Campos, Mod. Phys. Lett. A **31**, 1650066 (2016).
 - [14] C. Tsallis, Braz. J. of Phys. **39**, 337 (2009).
 - [15] N.G. Antoniou, F. Diakonov and C.G. Papadopoulos, Phys. Lett. B **265**, 399 (1991).
 - [16] N.G. Antoniou, V.E. Zambetakis, F.K. Diakonov and N.K. Diakonou, Z. Phys. C **55**, 631 (1992).
 - [17] N.G. Antoniou, F. Diakonov, I.S. Mistakidis and C.G. Papadopoulos, Phys. Rev. D **49**, 5789 (1994).
 - [18] N.G. Antoniou, N. Davis and F.K. Diakonov, Phys. Rev. C **93**, 014908 (2015).
 - [19] A. Bialas, Nucl. Phys. A **545**, 285c (1992).
 - [20] A. Bialas, Acta Phys. Pol. B **23**, 561 (1992).
 - [21] M. Froissart, Phys. Rev. **123**, 1053 (1961).
 - [22] L. Lukaszuk and A. Martin, Nuovo Cim. A **52**, 122 (1967).
 - [23] A. Martin, Phys. Rev. D **80**, 065013 (2009).
 - [24] T.T. Wu, A. Martin, S.M. Roy and V. Singh, Phys. Rev. D **84**, 025012 (2011).
 - [25] A. Martin and S.M. Roy, Phys. Rev. D **91**, 076006 (2015).
 - [26] V. A. Okorokov, arXiv: 1805.10514 [hep-ph] (2018).
 - [27] A. Rényi, in *Proceedings of the IV Berkeley Symposium on mathematical statistics and probability* **1**, 547 (1960).
 - [28] C. E. Shannon, Bell Sys. Tech. J. **27**, 379 (1948).
 - [29] S. Abe, Phys. Lett. A **224**, 326 (1997).
 - [30] C. Beck, Contemporary Phys. **50**, 495 (2009).
 - [31] C. Tsallis, *Introduction to nonextensive statistical mechanics: approaching a complex world*. Springer Science (2009).
 - [32] Sh. F. Y. Liu and R. Rapp, arXiv: 1501.07892 [hep-ph] (2015).
 - [33] V. Barone and E. Predazzi, *High-energy particle diffraction*. Springer-Verlag (2002).
 - [34] C. Patrignani *et al.* (Particle Data Group), Chin. Phys. C **40**, 100001 (2016).
 - [35] E. Eichten, K. Gottfried, T. Kinoshita, K. D. Lane, and T.-M. Yan, Phys. Rev. D **17**, 3090 (1978).
 - [36] A. P. Trawiński *et al.*, Phys. Rev. D **90**, 074017 (2014).
 - [37] S. Bethke, Eur. Phys. J. C **64**, 689 (2009).
 - [38] G. Grunberg, Phys. Lett. **95B**, 70 (1980).
 - [39] G. Aad *et al.* (ATLAS Collaboration), Phys. Rev. D **86**, 014022 (2012); V. Khachatryan *et al.* (CMS Collaboration), Eur. Phys. J. C **75**, 288 (2015).
 - [40] V. Khachatryan *et al.* (CMS Collaboration), Eur. Phys. J. C **75**, 186 (2015).
 - [41] E. K. G. Sarkisyan and A. S. Sakharov, Eur. Phys. J. C **70**, 533 (2010); E. K. G. Sarkisyan, A. N. Mishra, R. Sahoo and A. S. Sakharov, Phys. Rev. D **93**, 054046 (2016).
 - [42] J. Bartels and M.A. Braun, arXiv: 1711.04703 [hep-th] (2017).
 - [43] D. Bohm, Phys. Rev. **85**, 166 (1952); *ibid*, 180 (1952).